Modeling Reverse Iontophoresis for Noninvasive Glycemic Monitoring

BEE 4530
Computer-Aided Engineering: Applications to Biomedical Processes
May 14, 2015

Group 5
Stephanie Cheng
Esra Kuehlert
Latha Panchap
Kathleen Young

Table of Contents

I. Executive Summary

Current methods of glucose monitoring for diabetics are invasive and require blood to be drawn. Despite improved technologies for self-monitoring glucose, patient adherence for these methods is low due to the inconvenience and complexity of the regimen. Several iterations of noninvasive devices have been developed for monitoring glucose levels, but these devices still require direct blood glucose analysis for calibration purposes. Therefore, a current focus in diabetes research is developing standalone noninvasive methods that do not require direct measurements. Although still in the proof-of-concept phase, a promising alternative to current treatments is a temporary tattoo glucose sensor.

This glucose monitoring system consists of a removable device in the form of a decal-style temporary tattoo with an electrochemical sensor. The sensor has two electrodes that apply a voltage to the skin that brings glucose to the surface, a concept known as *reverse iontophoresis*. In reverse iontophoresis, ions flow diffusively in the medium in the direction opposite of the current resulting from the applied voltage. In the glucose sensor, the movement of sodium ions towards the cathode creates an osmotic pressure gradient. This pressure gradient drives water to the cathode, bringing interstitial glucose along to the cathode. At the cathode, the glucose reacts with glucose oxidase, transducing the glucose concentration into a measurable visual signal.

Research on non-invasive glucose monitoring is still very much in its nascent stage. This project seeks to enhance the current understanding of the coupled physics behind the glucose monitoring process, as this has yet to be established. There is little modeling on the physics of any glucose monitoring system, despite their existence for the past 20 years. Published research mainly focuses on direct glucose measurements or signal correlations rather than describing the physical processes involved.

The model described in this report focuses on defining the coupling of the different physics in the glucose sensor, and does not simulate the visual signal for the glucose level reading. The main goal was to optimize the design of a proof-of-concept glucose sensor described by Bandodkar, et al. in 2015. We validated our model by comparing our extracted glucose values to experimental values reported by Ching, et al. in 2008. Our final extracted glucose values were consistently within the range of their trial results, suggesting that our model closely mimicked experimental results. From our sensitivity analysis, we found that our model was most sensitive to glucose diffusivity, initial glucose concentration, and the reactive flux. However, it was not very sensitive to the parameters that we wanted to use to optimize the design: voltage and inter-electrode distance. We determined that this was because diffusion through the skin occurred slower than the reactive flux boundary extracted glucose, creating a diffusive shell around the cathode.

Further work on our model will involve understanding and optimizing the reactive flux boundary, such that we minimize the presence of the diffusive shell. Additionally, the model will incorporate the glucose oxidase-containing gel layer between the skin surface and electrodes and the conversion of the extracted glucose into a measurable signal for glucose monitoring.

II. Introduction

Background on Current Glucose Monitoring Methods

Diabetes is one of the most prevalent degenerative diseases in the world. As of 2014, it affects about 29.1 million people in the United States, with an estimated 8.1 million of those undiagnosed (Centers for Disease Control and Prevention, 2014). Although there are many types of diabetes, all require careful, regular monitoring of blood glucose levels. Currently, all self-testing methods require blood samples from painful and inconvenient finger pricks. Even self-described and FDA approved non-invasive testing methods are not truly noninvasive as they still require accompanying blood glucose testing from finger pricks. These noninvasive devices are still not consistently accurate enough for patients to rely on them entirely (U.S. Food and Drug Administration, 2013). Patient compliance with glucose monitoring is, therefore, a major concern, with an estimated 67% of diabetic patients failing to routine their blood glucose levels (Burge, 2001).

Although many products measure subcutaneous glucose levels, they are often not as accurate as direct blood glucose levels. Therefore, every noninvasive technique requires the drawing of blood for calibration. Researchers are currently investigating methods of measuring glucose levels without the need for directly measuring blood glucose levels.

Research Review on Reverse Iontophoresis

An emerging concept in glucose monitoring is the measurement of subcutaneous glucose levels in the interstitial fluid through reverse iontophoresis (Kovatchev, Shields, & Breton, 2009). Reverse iontophoresis is the electroosmotic transport of a solute to the voltage source as a result of an applied current. Since glucose is a large, neutral molecule, glucose cannot be directly transported when a current is applied because it is uncharged. Glucose molecules rely on osmotic forces for directed movement; and their movement has to be coupled to the transport of another solute. In this case, sodium ions are transported to the cathode. This buildup of sodium ions at the cathode creates a concentration gradient, and forces fluid to flow to the cathode iern or to dilute the salt concentration. It is this fluid flow which moves glucose to the cathode, where glucose undergoes an oxidation reaction by glucose oxidase. The release of electrons from this reaction is what provides the measurable signal.

GlucoWatch is a glucose monitor that utilizes reverse iontophoresis. The original GlucoWatch was on the market in 2002, but it was ultimately removed from consumer use due to skin irritation caused by the applied current. Newer iterations of the GlucoWatch have since been FDA approved and released on the market (U.S. Food and Drug Administration, 2013).

Other types of reverse iontophoresis glucose monitors include implanted glucose sensors used in continuous glucose monitoring (CGM). A tiny sensor is placed underneath the skin to monitor interstitial glucose levels, and is replaced within a couple of days. A transmitter then sends

the data to be converted into a reading. Patients must still confirm glucose levels with a standard blood glucose meter, as CGM devices are not as accurate and reliable as standard blood glucose meters (U.S. Department of Health and Human Services, 2013).

Current Research on Glucose Monitoring

Current research is focused on creating noninvasive glucose meters to monitor glucose levels without the need for accompanying finger pricks. One approach is to develop a glucose meter within a temporary tattoo (Bandodkar, et al., 2015). These tattoo sensors would be inexpensive and easily disposable, making them readily affordable and user-friendly. They would have to be replaced daily, but the expected cost of a few cents means that this would still be a very affordable solution. Glucose concentration profiles through interstitial fluid due to reverse iontophoresis has never been characterized before, and our sensor model below has helped further this research.

Problem Statement

We propose the development and optimization of a computational model that accurately represents the transport phenomena observed in the measurement of glycemic levels in the skin through reverse iontophoresis.

Design Objectives

1. Develop a COMSOL computational model for iontophoretic transport of sodium ions, water, and interstitial glucose in the skin to a cathode placed on the skin ("reverse iontophoresis") that accurately describes how this phenomenon occurs *in vivo.*
2. Optimize the design of the tattoo-based glucose sensor to maximize the glucose reading. Parameters to optimize include applied voltage and inter-electrode distance.

II. Schematics

The proof-of-concept paper by Bandodkar et al. in 2015 provided a design (Fig. 1) for the electrodes and sensor that we simplified for the purposes of modeling the reverse iontophoresis process, which is the principle process by which our monitor functions.

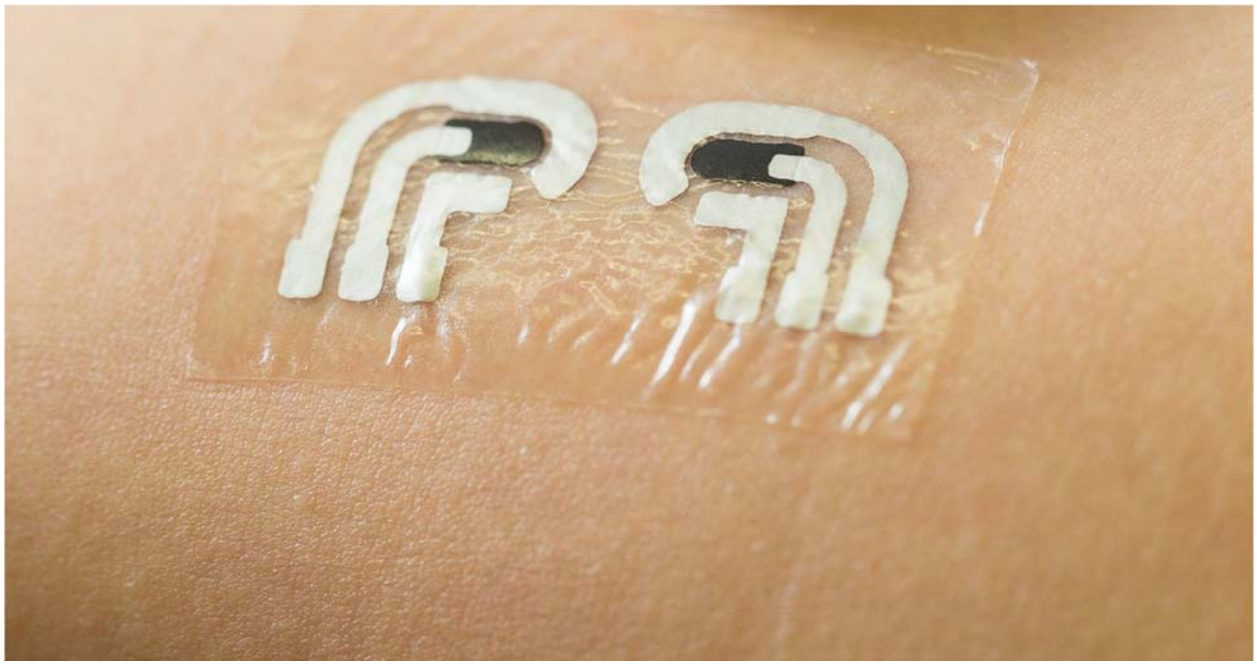

Figure 1. The prototype tattoo-based glucose sensor reported by Bandodkar et al. The physical configuration of this sensor informed the design of the modeling geometry in Figure 2.

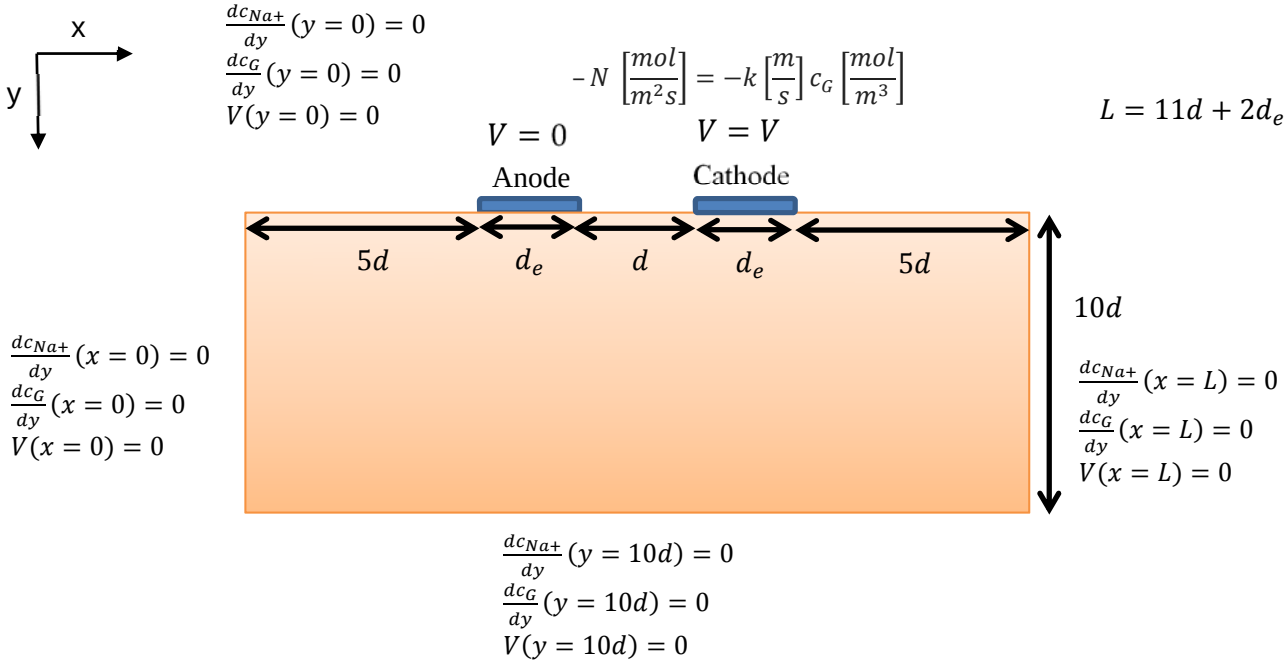

Figure 2. Problem schematic. Electrodes are placed on the skin, the domain of interest. The dimensions of our schematic will vary based on the distance between the electrodes. After talking with Professor Doerschuk of the Electrical and Computer Engineering and Biomedical Engineering Departments, we decided that ten times this distance would work as a reasonable boundary at which there would be no flux.

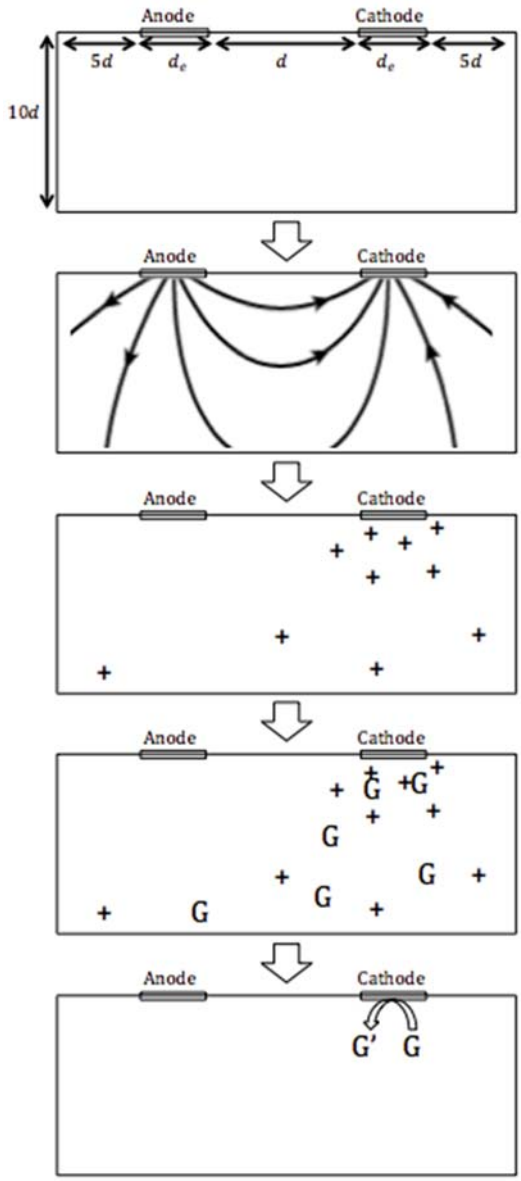

Figure 3. Illustration of steps involved in reverse iontophoresis transport of glucose. Initially, a mild current is applied to the electrodes, which creates an electric field into the skin and tissue. The positively charged sodium ions move towards the negatively charged cathode through electromigration. The ion gradient creates an osmotic pressure gradient that drives interstitial fluid towards the cathode, carrying dissolved glucose with it, also through electroosmosis. Glucose oxidase reactions at the cathode transduces the glucose concentration into a readable signal.

III. Methods

The governing equations and boundary conditions describe the various, highly coupled physics in our model. A current is applied to the skin through the electrodes, which creates an electric field into the skin and tissue. This causes the positively charged sodium ions to move towards the negatively charged cathode through electromigration. The ion gradient concentration at the cathode creates an osmotic pressure gradient that drives interstitial fluid towards the cathode,

carrying dissolved glucose with it again through electroosmosis. Glucose oxidase reactions at the cathode convert glucose into gluconic acid and, ultimately, hydrogen peroxide. These products induce a readable signal for glucose quantification purposes (not included in our model).

Table 1. Nomenclature of variables and input parameters of our model.

Parameter	Definition	Value	Units	Source
a	average radius of the pores	2.90E-9	m	(Ghosh & Blankschtein, 2007)
c_G	Concentration of glucose	---	mol/m^3	---
$c_{G,i}$	Initial concentration of glucose	4.72	mol/m^3	(Zakopoulos, et al., 2008)
c_{Na^+}	Concentration of sodium ions	---	mol/m^3	---
$c_{Na^+,i}$	Initial concentration of sodium	134.6	mol/m^3	(Fogh-Andersen, Altura, & Siggaard-Andersen, 1995)
D_G	Diffusivity of glucose	2.64E-10	m^2/s	(Khalil, Kretsos, & Kasting, 2006)
D_{Na^+}	Diffusivity of sodium ions	5.26E-10	m^2/s	---
F	Faraday's constant	9.65E4	C/mol	---
$\boldsymbol{i}$	current density vector	---	A/m^2	---
k_{GOx}	Glucose oxidase catalytic rate constant	735[s^{-1}]*d_e	m/s	(Kurnik, Berner, Tamada, & Potts, 1998)
$\boldsymbol{N_G}$	Flux vector of glucose	---	mol/m s	---
$\boldsymbol{N_{Na^+}}$	Flux vector of sodium ions	---	mol/m s	---
p	Counter-pressure driven flow gradient from osmotic pressure	---	Pa	---
R	Universal gas constant	8.314	J/mol K	---
T	temperature	310	K	---
$\boldsymbol{u}$	velocity vector	---	m/s	---
u_{m,Na^+}	Mobility of sodium ions	---	mol m^2/J s	---
V	Voltage potential	---	V	---
V_1	Applied voltage at cathode	-0.1	V	(Bandodkar, et al., 2015)
z_{Na^+}	Sodium ion charge number	1	---	---
ε_p	porosity	2.50E-5	---	(Tezel, Sens, & Mitragotri, 2003)
ε_w	Permittivity of the fluid	7.1E-10	F/m	(Cooper, 1999)
ζ	Zeta potential	0.023	V	(Morykwas, Thornton, & Bartlett, 1987)
κ	Conductivity	1.25E-5	S/m	(Miklavcic, Pavselj, & Hart, 2006)
λ	Van't Hoff Factor	1	---	---
μ	Viscosity of interstitial fluid	0.0035	Pa s	(Yao, Li, & Ding, 2012)
Π	Osmotic pressure	---	Pa	
ρ	Density of interstitial fluid	1000	kg/m^3	(Yao, Li, & Ding, 2012)
τ	Tortuosity of the porous structure	10	---	---

Governing Equations

Our model involves the interaction of voltage and diffusion of the species of interest. A steady state voltage equation (1) describes the electric field throughout the skin as a result of current applied at the electrodes. This external applied field causes the transport of charged species; sodium ions diffuse towards the cathode as a result.

Voltage equation $$\frac{d^2V}{dx^2} + \frac{d^2V}{dy^2} = 0 \quad (1)$$

To maintain osmotic equilibrium, interstitial fluid with dissolved glucose flows toward the cathode. The transport of sodium and glucose depend on osmotic pressure and concentration gradients. As mentioned earlier, sodium transport is also influenced by the application of an external electric field. We modified osmotic pressure to include the concentrations of both sodium and glucose.

Osmotic pressure $$\Pi = \lambda(c_{Na+} + c_G)RT \quad (2)$$

Both the voltage (1) and osmotic pressure (2) contribute to the velocity field equation.

Velocity field $$\boldsymbol{u} = -\frac{\varepsilon_p a^2}{8\mu\tau}\nabla(p - \Pi) + \frac{\varepsilon_p \varepsilon_w \zeta}{\mu\tau}\nabla V \quad (3)$$

The Nernst-Planck flux equations for sodium and glucose are dependent on the velocity field (3) and concentration gradients. The Nernst-Planck fluxes (4a) and (4b) describe the transport of ions through fluid due to both a concentration gradient and an applied electric field, where $u_{m,Na^+} = \frac{D_{Na+}}{RT}$. Glucose is not directly affected by applied electric fields because it is a neutral solute.

Nernst-Planck fluxes of sodium and glucose

$$\boldsymbol{N_{Na^+}} = -D_{Na^+}\nabla c_{Na^+} - z_{Na+}u_{m,Na+}Fc_{Na+}\nabla V + c_{Na+}\boldsymbol{u} \quad (4a)$$

$$\boldsymbol{N_G} = -D_G\nabla c_G + c_G\boldsymbol{u} \quad (4b)$$

Finally, equations (5a) and (5b) describe the time-dependent mass transport of within the domain.

Concentration profiles of sodium and glucose

$$\frac{\partial c_{Na+}}{dt} + \nabla \boldsymbol{N_{Na+}} = 0 \quad (5a)$$

$$\frac{\partial c_G}{dt} + \nabla \boldsymbol{N_G} = 0 \quad (5b)$$

Boundary Conditions

The boundary conditions provide the context for the equations used in the model. They provide the different physical limits the model has to follow. From the first physics where voltage/equivalent current is applied across the electrodes, the boundary condition will reflect some constant voltage/current. Due to the high resistance of air, the current will only flow through the skin. This means that at the skin/air boundary, there is no normal current.

As the applied electric field is very small in comparison to the arm, and becomes weaker further away from the electrodes, a semi-infinite model can be assumed for the right, left, and bottom boundaries for voltage. Since the voltage is only applied at the electrodes, all other boundaries therefore have no voltage flux. At the anode surface, the voltage $V = 0$ and at the cathode surface, $V = V_1$.

After the voltage is applied, sodium ions are directly affected. There is assumed to be no sodium ion flux at the bottom ($\frac{dc_{Na+}}{dy}(y = 10d) = 0$), left ($\frac{dc_{Na+}}{dx}(x = 0) = 0$), and right ($\frac{dc_{Na+}}{dx}(x = L) = 0$) boundaries, far from the effects of the voltage field. Sodium ions are not able to flow through the skin into the air, and therefore there is no sodium ion flux at the top boundary ($\frac{dc_{Na+}}{dy}(y = 0) = 0$).

As sodium builds up at the cathode, glucose is transported. The boundary conditions for glucose have to be defined. Glucose molecules have no flux at the bottom ($\frac{dc_G}{dy}(y = 10d) = 0$), left ($\frac{dc_G}{dx}(x = 0) = 0$), or right boundaries ($\frac{dc_G}{dx}(x = L) = 0$) far from the electrodes. There is no flux at the top boundary ($\frac{dc_G}{dy}(y = 0) = 0$) as glucose cannot flow through the skin into the air. At the cathode, glucose reacts with glucose oxidase to form gluconic acid and hydrogen peroxide. This is considered a reactive flux boundary and can be modeled using the relationship,
$-N\left[\frac{mol}{m^2 s}\right] = -k\left[\frac{m}{s}\right] c_G[\frac{mol}{m^3}]$.

Initial Conditions

At the start of the modeling process when time t = 0, there is no current anywhere within the interstitial fluid ($\frac{di}{dx}(t = 0) = 0$). Sodium ions are at a baseline concentration throughout the interstitial fluid at time ($c_{Na^+}(t = 0) = constant$). Glucose is at some constant concentration throughout the interstitial fluid ($c_G(t = 0) = constant$).

IV. Results and Discussion

Our model was run for 600 seconds (10 minutes) to match the *in vivo* experiments performed by Bandodkar et al. The results of the voltage distribution, sodium concentration, and glucose concentration throughout the domain are discussed below.

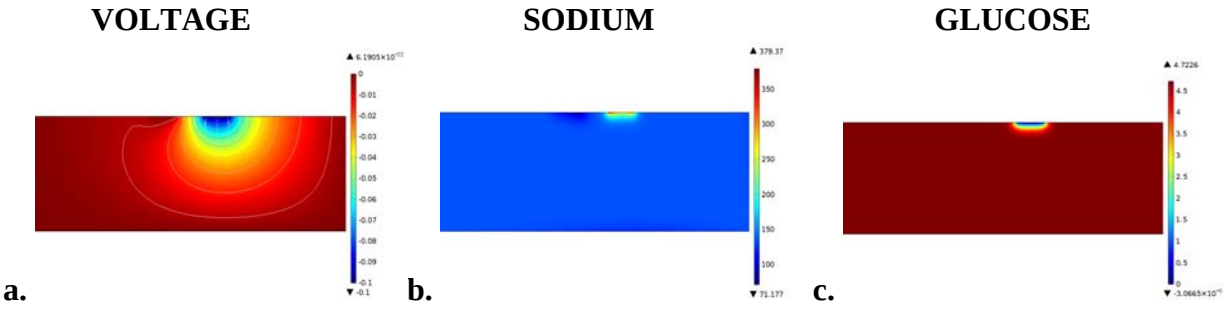

Figure 4. COMSOL surface plots of the a) voltage, b) sodium concentration, and c) glucose concentration throughout the domain after 600 seconds (final computation time).

All plots depict the variable behavior throughout the domain after 600 seconds of computation. The voltage surface and contour plot in the left-most figure depict voltage field. The center figure depicts the concentration of sodium throughout the domain. The majority of the domain remains at the initial concentration of 134.6 mol/m^3. The glucose concentration profile in the right figure depicts the concentration of glucose throughout the domain. The majority of the domain remains at the initial concentration of 4.72 mol/m^3. Due to the high catalytic rate constant, the flux of glucose out of the domain at the cathode is very high. Glucose appears to be depleted to a small concentration at the cathode due to the reactive flux.

Validation

To validate our model, we compared our model against experimental results obtained by Ching et al. (2008) as shown in Figure 5. We implemented the model with geometry relevant to the Ching paper: 23 mm between the electrode centers, polarity reversal of applied voltage every 15 minutes for 60 minutes, and decreased reactive flux constant. Experimentally extracted glucose levels differed from our model by 3.0% and -3.6% for Electrodes 1 and 2, respectively, showing that our model closely captures physical results. From this, we reasoned that our model can be used to accurately predict glucose extraction in real life.

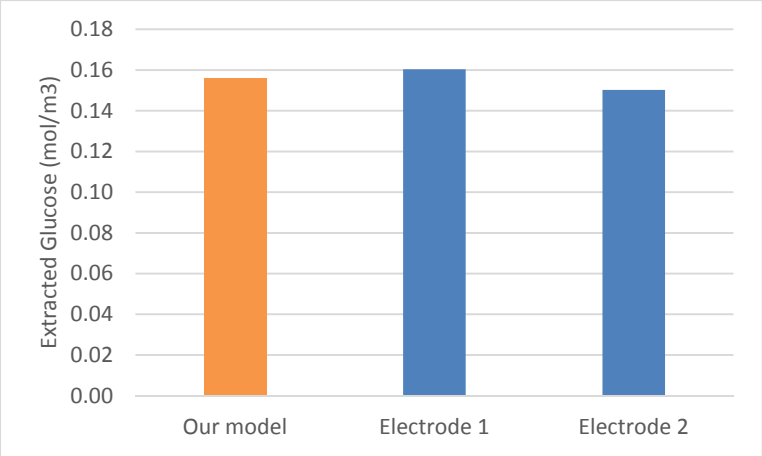

Figure 5. Comparison of extracted glucose concentrations computed by our model and experimentally derived by Ching et al. in 2008. Electrode 1 and 2 represent two different trials performed.

Sensitivity Analysis

The parameters evaluated for sensitivity analysis were zeta potential, average pore radius, ISF density, initial glucose concentration, applied voltage, glucose oxidase reactive flux constant, and glucose and sodium diffusivities. A large number of parameters were evaluated because this model has not previously been implemented, to our knowledge. Therefore, we sought to test the sensitivity of the model to many of parameters that may affect glucose transport. To quantify the sensitivity analysis, the total extracted glucose over time at the cathode was computed for the aforementioned parameters.

- Zeta potential: The zeta potential value is an estimate from previous work (COMSOL, 2015) and is not verified within the literature. Because its true value is unknown, we needed to determine a range of zeta potential for which the model was valid.
- Average pore radius: In the initial stages of implementation, the solution would not converge. We found that average pore radius was the limiting factor, thus we suspected that average pore radius would significantly affect glucose extraction.
- ISF density: This value is estimated from the density of water, so we wanted to determine if this approximation affected glucose extraction.
- Initial concentration of glucose: Since there is a range of physiological initial glucose concentrations, we wanted to ascertain that our model would work as expected with different initial values.
- Voltage: Applied voltage is a significant parameter in our model and is known to directly affect the rate of iontophoretic transport. We performed sensitivity analysis to determine the relative effects of adjusting applied voltage on the amount of extracted glucose.
- Glucose oxidase reactive flux constant: The value used for the glucose reactive flux constant was reported by Kurnik et al. (1998). The reaction constant was given with

the units [s^{-1}], but our flux boundary required units of [m/s]. Therefore, we scaled the parameter by the length of the electrode. As this value was an approximation, sensitivity analysis was necessary to determine the influence of the flux constant

- Diffusivities of glucose and sodium: The sensitivity of diffusivity of glucose through the skin was examined as this parameter was particularly important to the results. The Diffusivity of sodium through the skin was proportioned to the diffusivity of glucose, based on their respectively diffusivities in water. Therefore, this was an approximation.

Figure 6 describes all the parameters that do not contribute to significant changes in the total extracted glucose level. Figure 6a demonstrates that over a zeta potential range of 0-5 V, the extracted glucose concentration changes minimally. The sensitivity values all resulted in values slightly less than the extracted glucose value generated from the zeta potential parameter used of 0.023 V. A zeta potential of 0 V has the smallest change at -1.5E-5%, while a zeta potential of 5 V has the greatest change at -0.070%. The values appear to suggest that the greater the difference between the zeta potential values used, the greater the sensitivity percentage change, although the change is still less than 1%.

Figure 6b also shows that the extracted glucose concentration does not appear to be particularly sensitive to average pore radius. An increase of 10% in the average pore radius has a greater change from the parameter value used to run the model than a decrease of 10% in the average pore radius (0.11% vs. 0.023%). This may be because a larger pore radius allows glucose to diffuse more easily to the cathode to be reacted.

Like with the zeta potential and average pore radius, changing the ISF density results in minor changes in the extracted glucose concentration, as seen in Figure 6c. Increasing the ISF density by 10% to 1010 kg/m^3 causes the extracted glucose to increase by 0.064%, while increasing by 20% to 1020 kg/m^3 decreases the extracted glucose by 0.045%. A 30% increase in the ISF density to 1030 kg/m^3 increases the extracted glucose by 0.018%. Again, these changes are miniscule as they are all less than even 0.1% from the ISF density value chosen for the model.

Varying voltage from -0.025 to -2 volts produces minimal changes in the extracted glucose level. The voltage parameter value used in the model was -0.1 volts, and we could not vary voltage to the physiological danger level of 25 volts due to the limited computing power. Changing the voltage within our range gave extracted glucose values that are slightly less than the one in our model. The percent change is either -0.0098% or -0.00051%, as displayed in Figure 6d.

Finally, Figure 6e shows that changing the sodium diffusivity, as with the rest of the parameters described above, does not produce significant changes in the extracted glucose levels. The direction of the change appears to alternate, with a 20% decrease, 10% decrease, 10% increase, and 20% increase in the sodium diffusivity resulting in a -0.015%, 0.065%, -0.025%, and 0.096%.

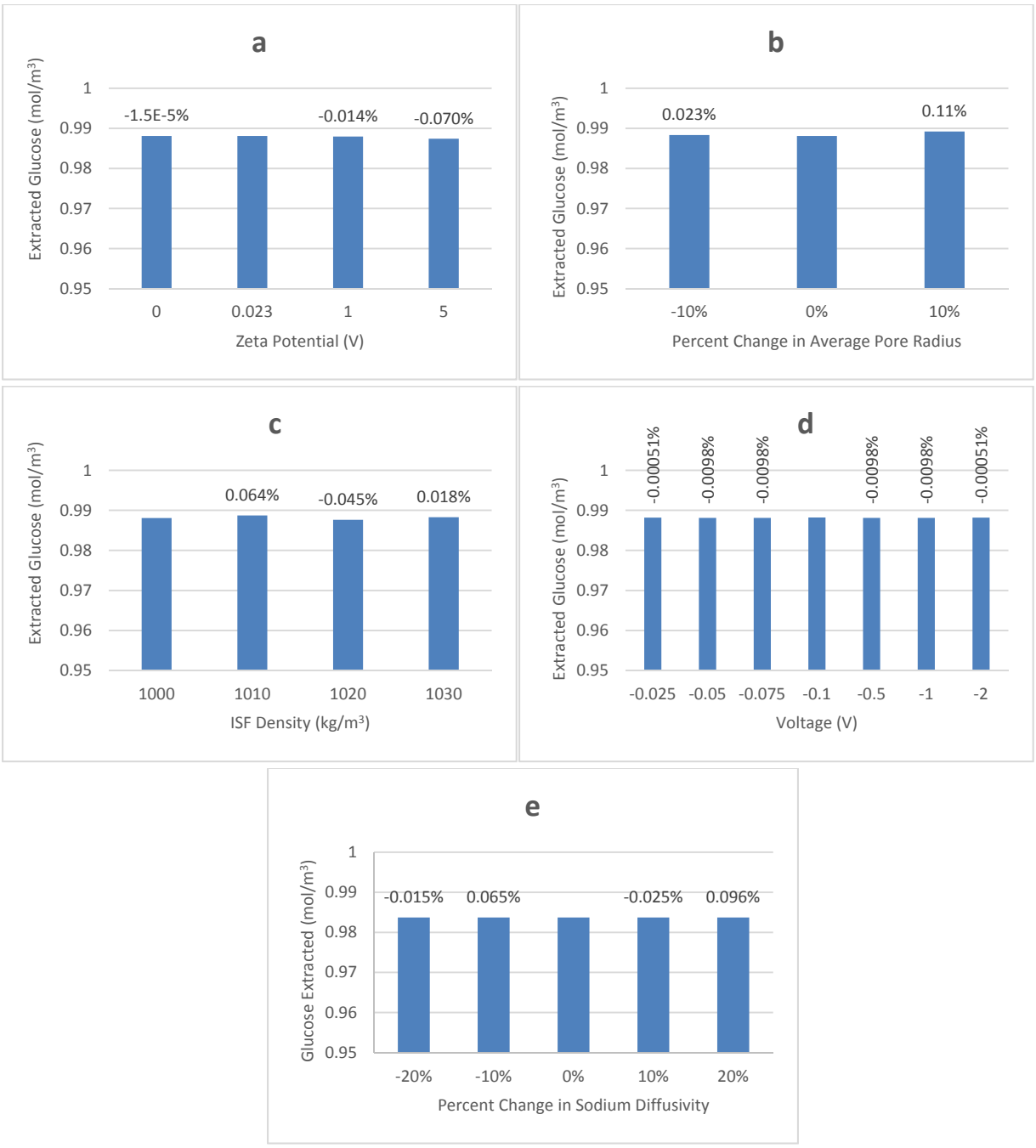

Figure 6. Total extracted glucose after 600 seconds for varying (a) zeta potential values, (b) average pore radii, (c) ISF densities, (d) voltages, and (e) sodium diffusivities. Note that the percent changes in extracted glucose are well below 1%.

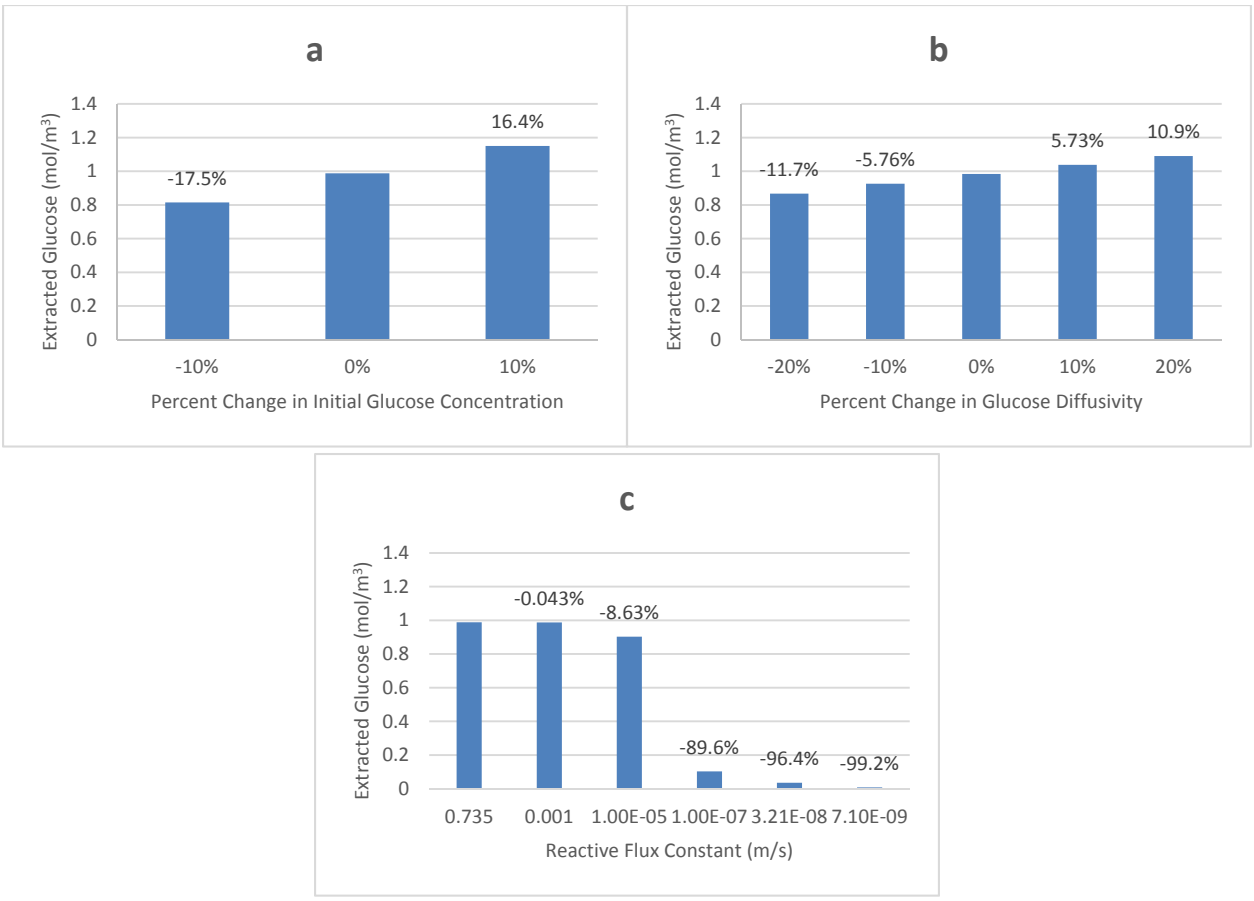

Figure 7. Total extracted glucose after 600 seconds for varying (a) initial glucose concentrations, (b) glucose diffusivities, and (c) reactive flux constants.

Figure 7 displays the parameters which cause much more relevant changes to total extracted glucose than those in Figure 6. Figure 8a shows how a 10% decrease and increase in the initial glucose concentration results in a 17.5% decrease and 16.4% increase in the extracted glucose levels, respectively. This is sensible as if the starting concentration of glucose is decreased, there would be less glucose diffusing to the cathode to be converted to gluconic acid. If the starting concentration of glucose is higher, then there would be more glucose to diffuse to the cathode and thus more total glucose extracted.

Similar to how the initial glucose concentration affects the extracted glucose levels, a decrease in the glucose diffusivity would decrease the amount of glucose transported to and reacted at the cathode as the glucose movement would be slower than usual. Less glucose would be able to arrive at the cathode during the same run time. Likewise, an increase in the glucose diffusivity would increase the amount of glucose transported to and reacted at the cathode due to the faster movement of glucose; this would allow more glucose to be converted for the same run time. Figure 7b follows this intuition as a 20% decrease, 10% decrease, 10% increase, and 20% increase results in a -11.7% decrease, -5.76% decrease, 5.73% increase, and 10.9% increase in the extracted glucose concentration. The values also show that as the difference increases between the sensitivity

glucose diffusivity value and the parameter value used in the model, the percent difference also increases.

Finally, Figure 7c shows that changes in the reactive flux constant can produce drastic changes in the extracted glucose values, but only when the parameter value is changed by many orders of magnitude. Changing the reactive flux constant from the model value of 0.735 m/s to 0.001 m/s only produces a -0.043% in extracted glucose at 600 seconds, whereas changing the value to 1E-5 m/s produces a -8.63% change. Changing the reactive flux constant by two more orders of magnitude to 1E-7 m/s produces a major change for a decrease of 89.6%. A reactive flux constant of 1E-9 m/s causes a decrease of almost all of the extracted glucose. The greatest percentage change occurs between a reactive flux constant of 1E-5 and 1E-7 m/s, where there is an 80.97% decrease.

Optimization

We implemented an optimization function that maximized the amount of extracted glucose over ranges of applied voltage and inter-electrode distance. This optimization function was calculated over varying electrode distances to produce a graph that optimizes the inter-electrode distance and voltage to produce the largest value of glucose.

We implemented simultaneous parametric sweeps of inter-electrode distance d (1, 1.5, 2, 2.5, 3, 3.5, 4, 4.5, 5, 5.5, 6 mm) and applied voltage V_1 (-0.01, -0.05, -0.075, -0.1, -0.5, -1, -2, -4 V). The maximum occurs at a combination of -0.075 V and 3.5 mm inter-electrode distance. However, the differences between this maximum and the extracted glucose at other combinations of voltage and inter-electrode distance are insignificant, with all combinations producing differences less than 1% from the solution run with original parameters in Table 1. The insignificance of this maximum led us to conclude that the sensor was not really optimized.

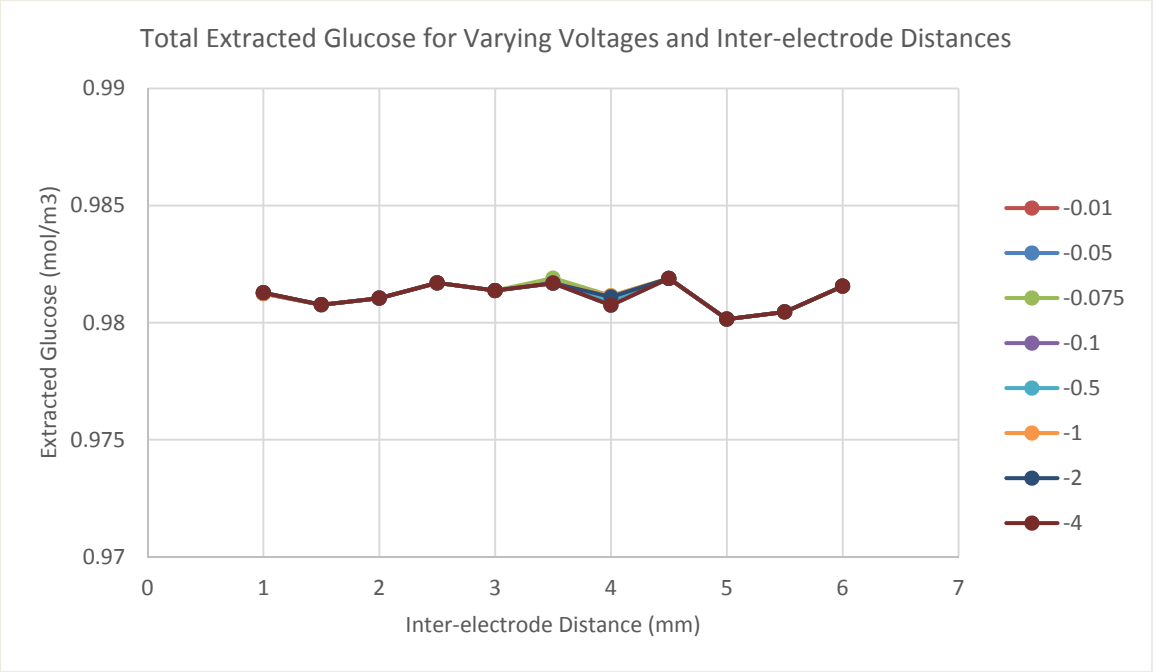

Figure 8. The total amount of glucose extracted (mol/m^3) after 600 seconds for combinations of inter-electrode distance (x-axis) and voltage (legend, in Volts).

The results shown in Figure 8 contradict our expectations. Inter-electrode distance and especially voltage magnitude should have significantly affected the amount of glucose extracted. This assumption is based on the principles of iontophoresis; increased voltage additionally increases the rate of iontophoretic transport. We predicted that this unexpected result is due to a diffusive shell created by the reactive flux at the cathode. Glucose in the surrounding area is depleted too quickly, and diffusive transport of glucose is unable to compensate for the lost glucose. Figure 9 shows that the diffusive flux is very high in a large region surrounding the cathode. In order to decrease the size of this bubble, we need to decrease the rate at which glucose is being depleted. This is best controlled by decreasing the reactive flux constant or the size of the electrode.

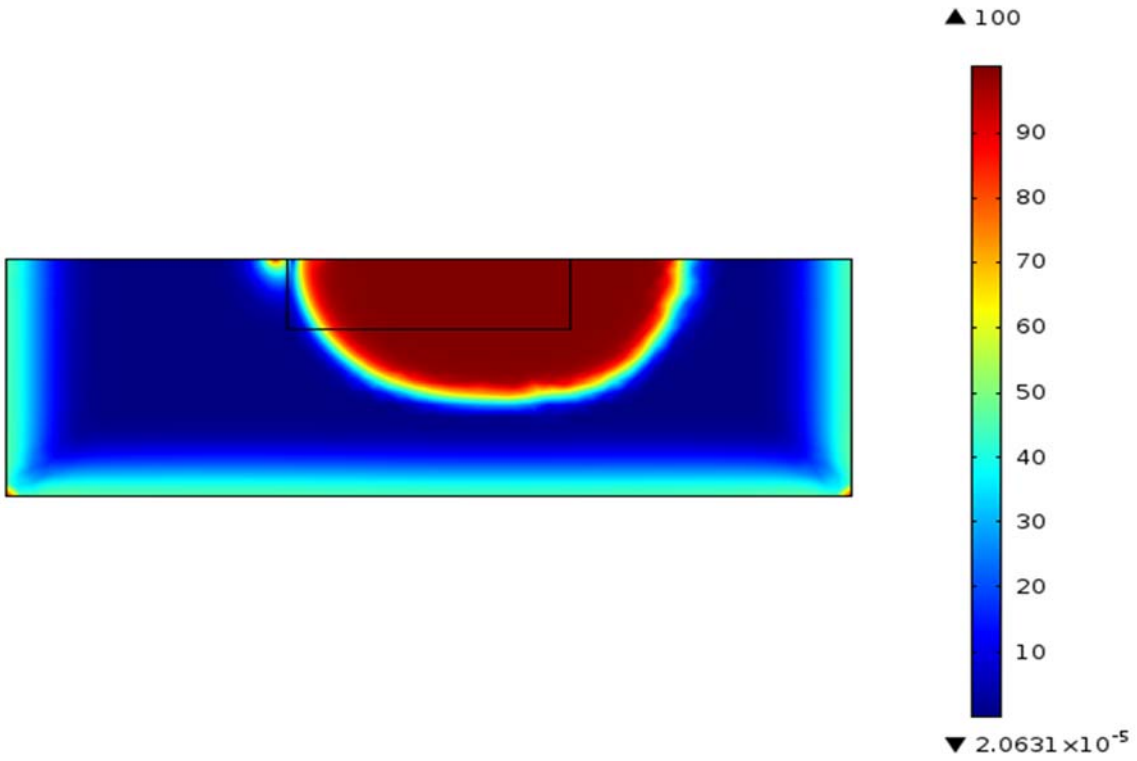

Figure 9. A surface plot of diffusive flux/total flux. This shows the diffusive flux bubble that forms due to the high reactive flux, impeding the movement of glucose to the cathode.

Conclusions and Design Recommendations

We designed and implemented a model of glucose transport via reverse iontophoresis in COMSOL to depict the physical processes occurring during extraction. We also aimed to optimize the design of this device to maximize the amount of glucose extracted from the skin. The results of our model showed the steady state voltage field created by the applied current with the highest gradient at the cathode, an accumulation of sodium at the cathode with slight repulsion at the anode, and a depletion of glucose at the cathode, due to the reactive flux boundary there. From our sensitivity analysis, we found that our model was most sensitive to glucose diffusivity, glucose initial concentration, and reactive flux. However, it was not very sensitive to the parameters that we wanted to use to optimize design: voltage and inter-electrode distance. We determined that this was because the reactive flux boundary extracted glucose faster than diffusion could replace, creating a diffusive shell around the cathode. We validated our model by comparing our extracted glucose values to those found in a study by Ching, et al. in 2008. To do so, we had to adjust the dimensions, running time, and reactive flux constant used in our model, resulting in an extracted glucose concentration that was very close to the experimental values.

Further work on our model would involve understanding and optimizing the reactive flux boundary such that we minimize the presence of the diffusive shell. This model would also

incorporate the glucose oxidase into a gel layer attached to the bottom of the electrode. We would model the conversion of the extracted glucose into a measurable signal for glucose monitoring. We noticed that some of the studies we used to validate our model had very different design parameters, including alternating current, different electrode shapes, and different domain sizes. We would also like to implement a 3D model to understand the effect of different current patterns and electrode areas and shapes on the amount of glucose extracted. This model could also include a representation of blood flow within the layer to understand the relationship between blood and interstitial glucose levels.

From our results, we were not able to optimize the design, finding instead that the applied voltage and distance between the electrodes did not significantly impact the amount of glucose extracted over 10 minutes. Further model development is required for design optimization applications, as higher voltages and smaller inter-electrode distances are expected to result in greater extracted glucose concentrations. It is important to recognize that as this model does not consider glucose transport at the cellular level, or the different diffusive rates through the skin layers, and is therefore more suitable for determining total extracted glucose, rather than the exact glucose concentration at a certain depth. Looking closely at electrode design, there are several design limitations that could come into play in addition to the inter-electrode distance and applied voltage. Electrodes can be made with a variety of metals, including copper, tungsten, silver, and brass. Each of these has a different electrical conductivity and heat capacity, which could lead to, at different levels of voltage and durations, slight increases in temperature of the device. This would be uncomfortable for the user and could lead to more serious health complications, such as burns. As such, design is limited by the materials available to create the electrodes and their properties. Additionally, the consistency of the hydrogel layer between the skin surface and the electrodes must allow the glucose to diffuse through to the electrodes as quickly as possible, such that the glucose diffusivity through the hydrogel does not delay the glucose oxidase reaction more than necessary.

V. Appendix A: Mathematical Statement of the Problem

The geometry/schematic is already included in the Introduction as Figure 2. The governing equations used are displayed below as well as in the Methods section.

A steady state voltage equation is used to describe the current and electric field. We assumed that there is a constant voltage applied that would not change over the course of the 10 minutes of the model.

Voltage equation $$\frac{d^2V}{dx^2} + \frac{d^2V}{dy^2} = 0 \quad (1)$$

To maintain osmotic equilibrium, interstitial fluid with dissolved glucose flows toward the cathode. The transport of sodium and glucose depend on osmotic pressure and concentration gradients. As mentioned earlier, sodium transport is also influenced by the application of an external electric field. We modified osmotic pressure to include the concentrations of both sodium and glucose.

Osmotic pressure $$\Pi = \lambda(c_{Na+} + c_G)RT \quad (2)$$

Both the voltage (1) and osmotic pressure (2) contribute to the velocity field equation.

Velocity field $$\boldsymbol{u} = -\frac{\varepsilon_p a^2}{8\mu\tau}\nabla(p - \Pi) + \frac{\varepsilon_p \varepsilon_w \zeta}{\mu\tau}\nabla V \quad (3)$$

The Nernst-Planck flux equations for sodium and glucose are dependent on the velocity field (3) and concentration gradients. The Nernst-Planck fluxes (4a) and (4b) describe the transport of ions through fluid due to both a concentration gradient and an applied electric field, where $u_{m,Na^+} = \frac{D_{Na^+}}{RT}$. Glucose is not directly affected by applied electric fields because it is a neutral solute.

Nernst-Planck fluxes of sodium and glucose

$$\boldsymbol{N_{Na^+}} = -D_{Na^+}\nabla c_{Na^+} - z_{Na+}u_{m,Na+}Fc_{Na+}\nabla V + c_{Na+}\boldsymbol{u} \quad (4a)$$

$$\boldsymbol{N_G} = -D_G\nabla c_G + c_G\boldsymbol{u} \quad (4b)$$

Finally, equations (5a) and (5b) describe the time-dependent mass transport of within the domain.

Concentration profiles of sodium and glucose

$$\frac{\partial c_{Na+}}{dt} + \nabla \boldsymbol{N_{Na+}} = 0 \quad (5a)$$

$$\frac{\partial c_G}{dt} + \nabla \boldsymbol{N_G} = 0 \quad (5b)$$

Our initial conditions show that at the start of the modeling process when time t = 0, there is no current anywhere within the interstitial fluid ($\frac{di}{dx}(t = 0) = 0$). Sodium ions are at a baseline concentration throughout the interstitial fluid at time ($c_{Na^+}(t = 0)$ = 134.6 kg/m^3. Glucose is at some constant concentration throughout the interstitial fluid ($c_G(t = 0) = 4.72$ mol/m^3.

Our boundary conditions show that that there is only voltage at the electrodes, such that at the anode surface, the voltage $V = 0$ and at the cathode surface, $V = V_1$. There is assumed to be no sodium ion flux at the bottom ($\frac{dc_{Na+}}{dy}(y = 10d) = 0$), left ($\frac{dc_{Na+}}{dx}(x = 0) = 0$), and right ($\frac{dc_{Na+}}{dx}(x = L) = 0$) boundaries, far from the effects of the voltage field. Sodium ions are not able to flow through the skin into the air, and therefore there is no sodium ion flux at the top boundary ($\frac{dc_{Na+}}{dy}(y = 0) = 0$). As sodium builds up at the cathode, glucose is transported. The boundary conditions for glucose have to be defined. Glucose molecules have no flux at the bottom ($\frac{dc_G}{dy}(y = 10d) = 0$), left ($\frac{dc_G}{dx}(x = 0) = 0$), or right boundaries ($\frac{dc_G}{dx}(x = L) = 0$) far from the electrodes. There is no flux at the top boundary ($\frac{dc_G}{dy}(y = 0) = 0$) as glucose cannot flow through the skin into the air. At the cathode, glucose reacts with glucose oxidase to form gluconic acid and hydrogen peroxide. This is considered a reactive flux boundary and can be modeled using the relationship, $-N\left[\frac{mol}{m^2 s}\right] = -k\left[\frac{m}{s}\right] c_G[\frac{mol}{m^3}]$.

The input parameters used in the model for the final solutions are described below in Table A1.

Table A1. Table of all of the input parameters used in the model.

Parameter	Definition	Value	Units	Source
a	average radius of the pores	2.90E-9	m	(Ghosh & Blankschtein, 2007)
c_G	Concentration of glucose	---	mol/m^3	---
$c_{G,i}$	Initial concentration of glucose	4.72	mol/m^3	(Zakopoulos, et al., 2008)
c_{Na^+}	Concentration of sodium ions	---	mol/m^3	---
$c_{Na^+,i}$	Initial concentration of sodium	134.6	mol/m^3	(Fogh-Andersen, Altura, & Siggaard-Andersen, 1995)
D_G	Diffusivity of glucose	2.64E-10	m^2/s	(Khalil, Kretsos, & Kasting, 2006)
D_{Na^+}	Diffusivity of sodium ions	5.26E-10	m^2/s	---
F	Faraday's constant	9.65E4	C/mol	---
$\boldsymbol{i}$	current density vector	---	A/m^2	---
k_{GOx}	Glucose oxidase catalytic rate constant	735[s^{-1}]*d_e	m/s	(Kurnik, Berner, Tamada, & Potts, 1998)
$\boldsymbol{N_G}$	Flux vector of glucose	---	mol/m s	---
$\boldsymbol{N_{Na^+}}$	Flux vector of sodium ions	---	mol/m s	---
p	Counter-pressure driven flow gradient from osmotic pressure	---	Pa	---
R	Universal gas constant	8.314	J/mol K	---
T	temperature	310	K	---
$\boldsymbol{u}$	velocity vector	---	m/s	---
u_{m,Na^+}	Mobility of sodium ions	---	mol m^2/J s	---
V	Voltage potential	---	V	---
V_1	Applied voltage at cathode	-0.1	V	(Bandodkar, et al., 2015)
z_{Na^+}	Sodium ion charge number	1	--	---
ε_p	porosity	2.50E-5	--	(Tezel, Sens, & Mitragotri, 2003)
ε_w	Permittivity of the fluid	7.1E-10	F/m	(Cooper, 1999)
ζ	Zeta potential	0.023	V	(Morykwas, Thornton, & Bartlett, 1987)
κ	Conductivity	1.25E-5	S/m	(Miklavcic, Pavselj, & Hart, 2006)
λ	Van't Hoff Factor	1	--	---
μ	Viscosity of interstitial fluid	0.0035	Pa s	(Yao, Li, & Ding, 2012)
Π	Osmotic pressure	---	Pa	
ρ	Density of interstitial fluid	1000	kg/m^3	(Yao, Li, & Ding, 2012)
τ	Tortuosity of the porous structure	10	--	

VI. Appendix B: Solution Strategy

In COMSOL, the solver used to solve the algebraic equations for Study 1 with the steady state voltage was MUMPS, while the solver used to solve the equations for Study 2 with the transient glucose and sodium concentrations was PARDISO. Time-stepping was not changed from the standard COMSOL settings. The relative tolerance for all solution variables was 0.01.

A plot of the free triangular mesh is shown in Figure B1. Figure B2 shows the point used for all mesh convergence analysis. Figures B3-5, along with Table B1, show the mesh convergence data for voltage, sodium concentration, and glucose concentration, the three independent variables in our model. We determined that convergence occurs for all three at a mesh size of 4050 elements. This corresponds to a maximum element size of 0.075 mm at the electrodes.

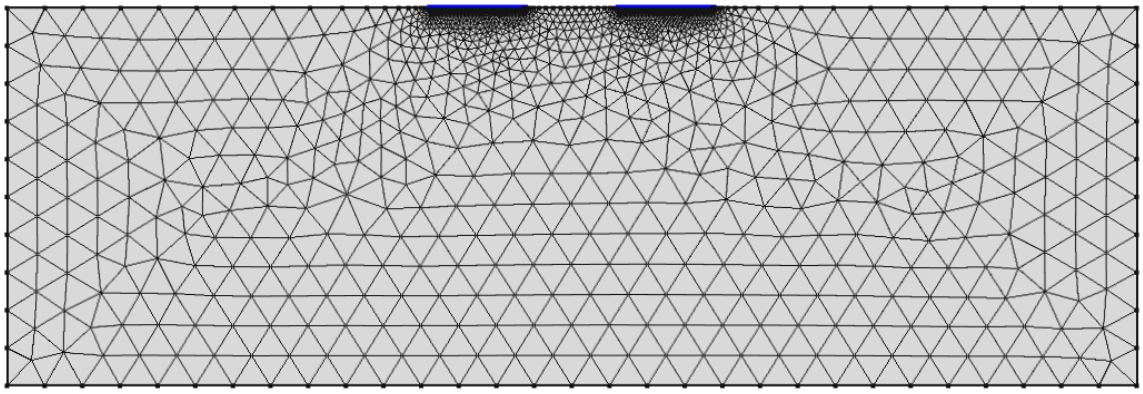

Figure B1. The mesh for our domain is depicted above. This is a free-triangular mesh with more dense distributions at the electrodes and between the electrodes. While performing the mesh convergence, we defined the max element size of the boundaries as 0.5 mm. The surface segment between the electrodes was defined at 0.5 mm for the max element size.

Table B1. Domain and boundary element counts retrieved from parametric sweep performed for mesh convergence for stationary solution for electric field and sodium and glucose concentrations).

Max Element Size (mm)	Domain Elements	Boundary Elements
1	1025	99
0.5	1019	99
0.1	1642	146
0.075	1941	167
0.050	2451	203
0.025	4099	313
0.015	6958	452
0.01	8760	624

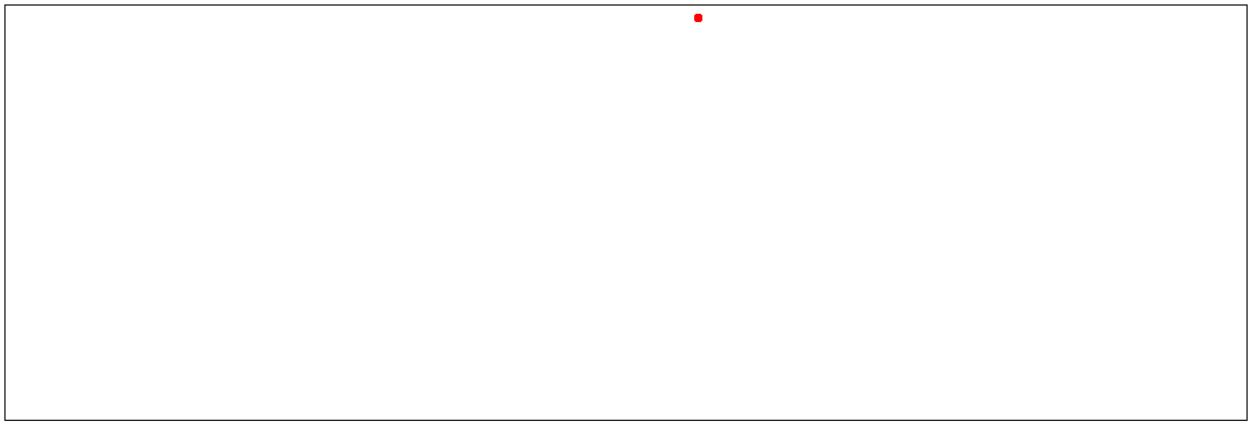

Figure B2. The point (1.8, 9.7) near the cathode in the domain where mesh convergence was tested for all variables.

The mesh convergences are displayed below in Figures B3-5. The parameters used to test for mesh convergence are voltage, sodium concentration, and glucose concentration as they are the three important, independent variables in our model.

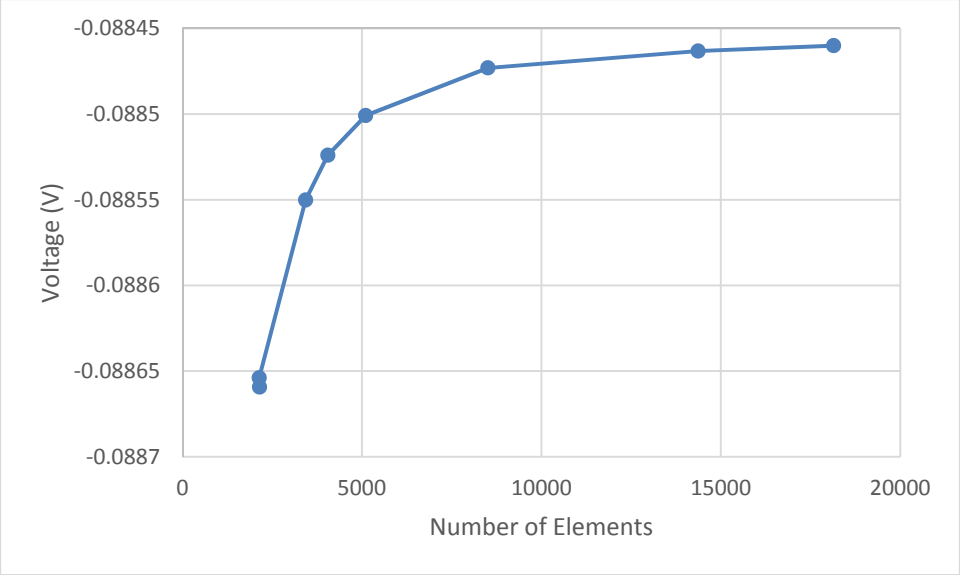

Figure B3. Voltage field mesh convergence at point (1.8, 9.7) near the cathode. Voltage convergence occurs at around 7000 elements. This is indicated by the noticeable plateauing of the voltage to a limiting value. It should also be noted that the voltage, plotted on the y-axis, is negative.

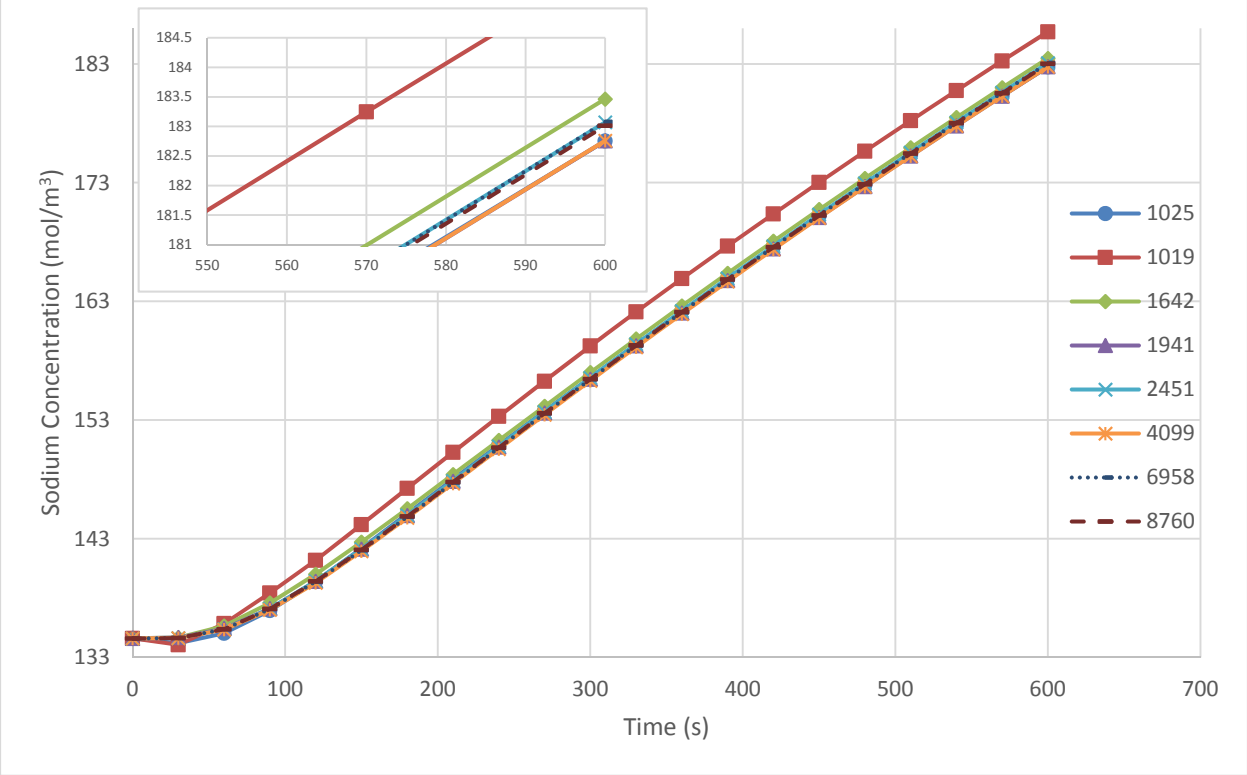

Figure B4. Sodium concentration mesh convergence at point (1.8, 9.7) near the cathode. Sodium convergence occurs with a max element size of 0.075 mm, which corresponds to 1941 domain elements.

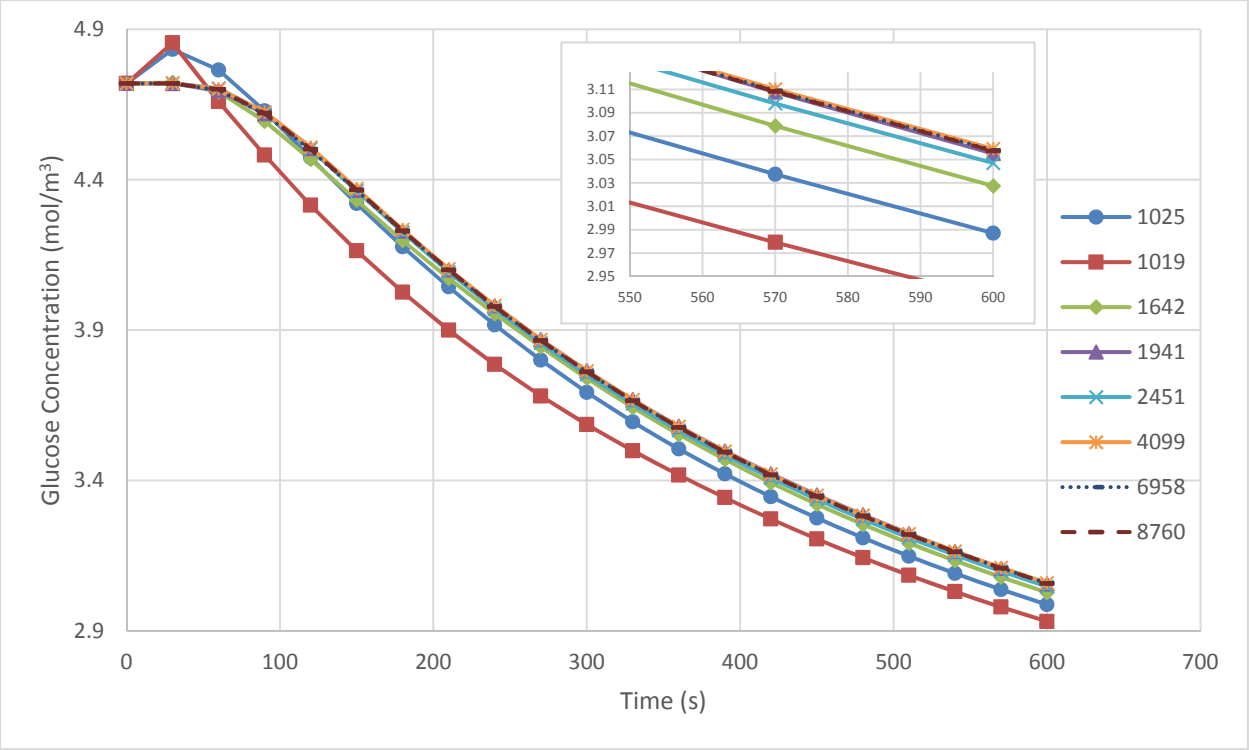

Figure B5. Glucose concentration mesh convergence at point (1.8, 9.7) near the cathode. Convergence of glucose concentration occurs by a max element size of 0.5 mm, which corresponds to 2451 domain elements.

VII. Appendix C: Additional Visuals

We additionally performed sensitivity analysis using sodium and glucose concentrations at a point 0.3 mm below the center of the cathode. Fig. C1 displays the results obtained for parametric sweeps of zeta potential and ISF density.

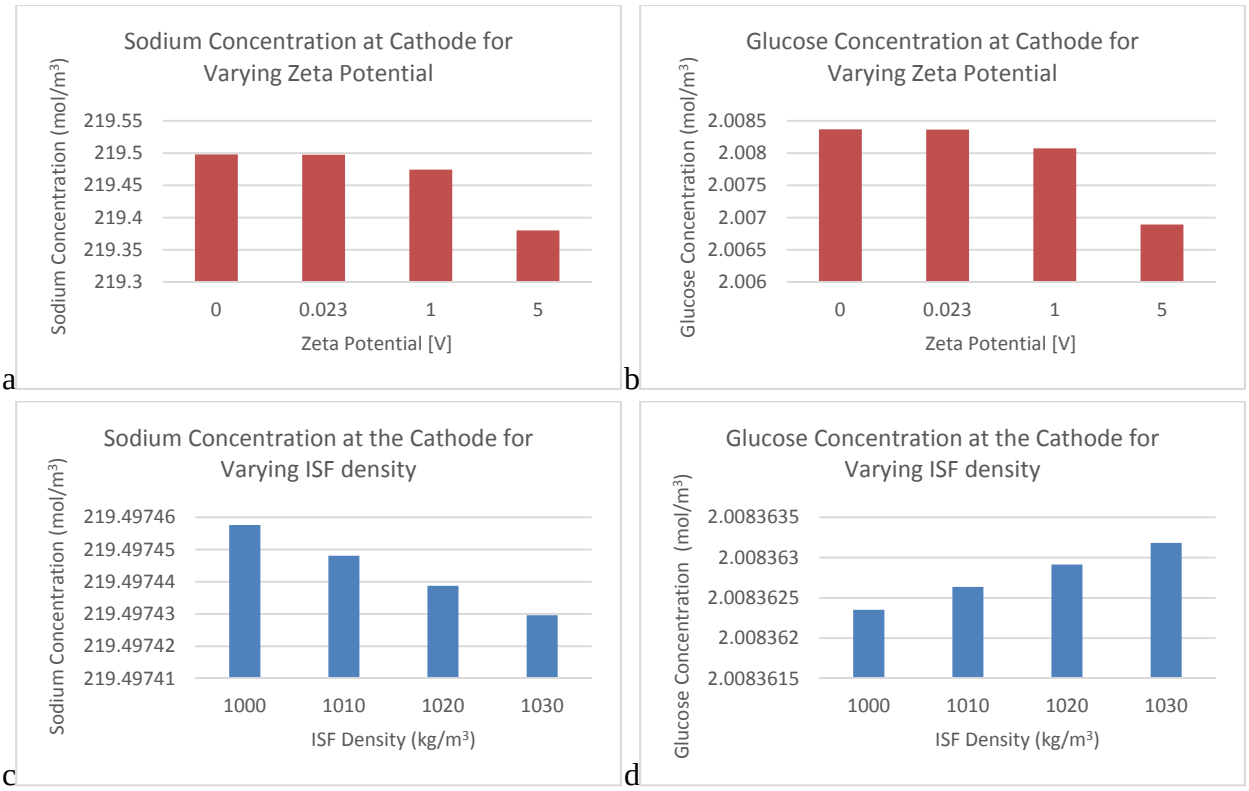

Figure C1. Sensitivity analysis performed for zeta potential and ISF density. To quantify sensitivity analysis initially, sodium and glucose concentrations at a point 0.3 mm below the center of the cathode were compiled.

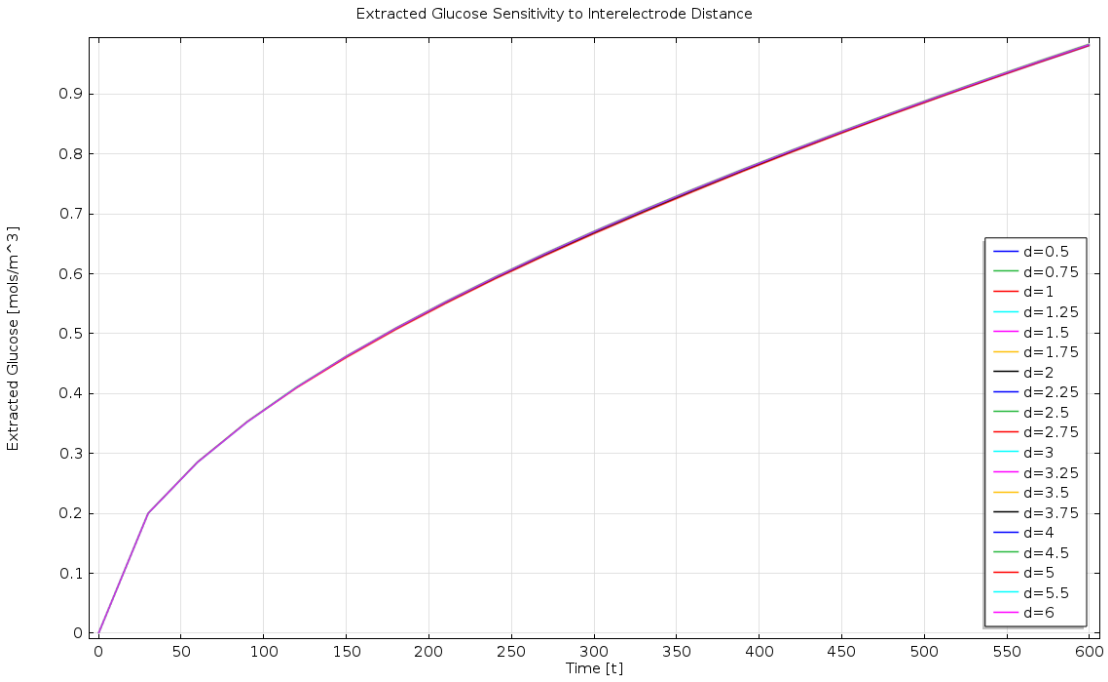

Figure C2. Sensitivity analysis parametric sweep of extracted glucose vs. inter-electrode distance d over time. This plot represents the data used to construct the sensitivity analysis plots. For all plots in the Results section, sensitivity analysis was performed on data points at the final time point of 600 s.

VIII. Appendix D: References

Bandodkar, A., Jia, W., Yardımcı, C., Wang, X., R. J., & Wang, J. (2015). Tattoo-Based Noninvasive Glucose Monitoring: A Proof-of-Concept Study. *Analytical Chemistry*, 394-398.

Burge, M. (2001). Lack of compliance with home blood glucose monitoring predicts hospitalization in diabetes. *Diabetes Care*, 1502-1503.

Centers for Disease Control and Prevention. (2014). *National Diabetes Statistics Report: Estimates of Diabetes and Its Burden on the United States, 2014.* Atlanta, GA: U.S. Department of Health and Human Services.

Ching, T., & Connolly, P. (2008). Simultaneous transdermal extraction of glucose and lactate from human subjects by reverse iontophoresis. *International Journal of Nanomedicine*, 211-223.

COMSOL. (2015). *Electro-osmotic Flow in Porous Media.* Retrieved from COMSOL Application Gallery: http://www.comsol.com/model/electroosmotic-flow-in-porous-media-11

Cooper, I. (1999, 2 17). *The University of Sydney School of Physics*. Retrieved from Electrical, Magnetic, and Optical Properties: Permittivity: http://www.physics.usyd.edu.au/teach_res/db/d0006c.htm

Delamater, A. (2006). Improving Patient Adherence. *Clinical Diabetes*, 71-77.

Fogh-Andersen, N., Altura, B., & Siggaard-Andersen, O. (1995). Composition of Interstitial Fluid. *General Clinical Chemistry*, 1522-1525.

Ghosh, S., & Blankschtein, D. (2007). Why is sodium cocoyl isethionate (SCI) mild to the skin barrier?--An in vitro investigation based on the relative sizes of the SCI micelles and the skin aqueous pores. *Journal of Cosmetic Science*, 229-244.

Kern, R. (2008). Sinker Electrode Material Selection. *EDM Today*, 1-6.

Khalil, E., Kretsos, K., & Kasting, G. (2006). Glucose Partition Coefficient and Diffusivity in the Lower Skin Layers. *Pharmaceutical Research*, 1227-1234.

Kovatchev, B., Shields, D., & Breton, M. (2009). Graphical and Numerical Evaluation of Continuous Glucose Sensing Time Lag. *Diabetes Technology & Therapeutics*, 139-143.

Kurnik, R., Berner, B., Tamada, J., & Potts, R. (1998). Design and Simulation of a Reverse lontophoretic Glucose Monitoring Device. *Journal of the Electrochemical Society*, 4119-4125.

Miklavcic, D., Pavselj, N., & Hart, F. (2006). Electrical Properties of tissues. *Wiley Encyclopedia of Biomedical Engineering*.

Morykwas, M., Thornton, J., & Bartlett, R. (1987). Zeta Potential of Synthetic and Biological Skin Substitutes: Effects on Initial Adherence. *Plastic & Reconstructive Surgery*, 732-739.

Tezel, A., Sens, A., & Mitragotri, S. (2003). Description of Transdermal Transport of Hydrophilic Solutes during Low-Frequency Sonophoresis Based on a Modified Porous Pathway Model. *Journal of Pharmaceutical Sciences*, 381-393.

U.S. Department of Health and Human Services. (2013, 10 4). *Continuous Glucose Monitoring*. Retrieved from National Diabetes Information Clearinghouse: http://diabetes.niddk.nih.gov/dm/pubs/glucosemonitor/index.aspx

U.S. Food and Drug Administration. (2013, 9 5). *Medical Devices*. Retrieved from Recently-Approved Devices: http://www.fda.gov/MedicalDevices/ProductsandMedicalProcedures/DeviceApprovalsandClearances/Recently-ApprovedDevices/ucm083294.htm

Yao, W., Li, Y., & Ding, G. (2012). Interstitial Fluid Flow: The Mechanical Environment of Cells and Foundation of Meridians. *Evidence-Based Complementary and Alternative Medicine*, 1-9.

Zakopoulos, N., Dolianitis, K., Theodorakis, M., Manios, E., Alevizaki, M., Stamatelopoulos, K., . . . Moulopoulos, S. (2008). Diurnal correlation of ambulatory blood pressure and interstitial glucose in patients with normal glucose tolerance. *Blood Pressure Monitoring*, 309-317.